Hydrolysis of a Lipid Membrane by Single Enzyme Molecules: Accurate Determination of Kinetic Parameters**

Michael Rabe, Seyed R. Tabaei, Henrik Zetterberg, Vladimir P. Zhdanov, and Fredrik Höök

Abstract: The accurate determination of the maximum turnover number and Michaelis constant for membrane enzymes remains challenging. Here, this problem has been solved by observing in parallel the hydrolysis of thousands of individual fluorescently labeled immobilized liposomes each processed by a single phospholipase A2 molecule. The release of the reaction product was tracked using total internal reflection fluorescence microscopy. A statistical analysis of the hydrolysis kinetics was shown to provide the Michaelis–Menten parameters with an accuracy better than 20% without variation of the initial substrate concentration. The combined single-liposome and single-enzyme mode of operation made it also possible to unravel a significant nanoscale dependence of these parameters on membrane curvature.

Many demanding challenges in bioscience and medicine can be uniquely addressed by a single-molecule approach.[1] Biological molecules of particular relevance in this context are enzymes, which are catalysts accelerating essential biochemical reactions with high efficiency and fidelity. When experiments are performed in the single-molecule regime, the concentration of the active enzyme becomes irrelevant for the determination of the specific enzymatic activity,[2] and simultaneously it is not necessary to synchronize the onset of catalytic activity of multiple enzymes. This approach has provided new insights on static and dynamic heterogeneities in enzymatic reactions,[3] fluctuations of catalytic reaction rates,[4] and conformational changes

during substrate conversion.[5] Parallel progress in structure determination and theoretical simulations has made the knowledge gained from single-molecule approaches of vital importance from fundamental scientific, medical diagnostic, and pharmaceutical points of view.[6]

Among the most important details of an enzymatic reaction are those quantifying the Michaelis–Menten steps, including the reversible association of substrate (S) and enzyme (E) into a substrate–enzyme complex (SE) and the catalytic formation of the product (P) [Eq. (1)].

$$S + E \rightleftharpoons SE \rightarrow P + E \tag{1}$$

For this scheme, the conventional mass-action law equations can easily be solved in the steady-state approximation for the SE concentration, and the reaction rate per enzyme is given by Equation (2).

$$W = \frac{k_1 k_{cat}[S]}{k_1[S] + k_{-1} + k_{cat}} = \frac{k_{cat}[S]}{[S] + K_m} \tag{2}$$

Here k_{cat} is the maximum turnover number, $K_m = (k_{-1} + k_{cat})/k_1$ is the Michaelis constant, and k_1 and k_{-1} are the rate constants for the reversible S–E association. Conventionally, these parameters are determined by repeated measurements of the initial conversion rate at varying substrate concentration.[5a] However, for enzymes that act on cell-membrane components[7] this procedure is not efficient because the substrate concentration cannot be readily varied.[8] Herein, we present measurements of single-enzyme membrane kinetics (Figure 1) and show how sufficient statistics enables extraction of both k_{cat} and K_m without the need to vary the initial substrate concentration.

The concept is shown for the membrane-active enzyme phospholipase A2 (PLA2), which catalyzes lipid digestion. For the phospholipid liposomes used here, this reaction occurs in the outer monolayer,[9] and the dye employed to visualize the process was positioned on the acyl chain of the phosphatidylcholine (PC) lysolipid product, proposed to be irreversibly released upon digestion.[10] Tail-labeled lipids of the same type as the major POPC lipid were chosen to minimize possible influence of the lipid composition on the reaction kinetics.[9]

The high-precision determination of k_{cat} and K_m was achieved by using large data sets obtained from a surface-based single-liposome assay that provides time-lapse microscopy images of surface-immobilized fluorescently labeled liposomes during their hydrolysis by single PLA2 molecule (Figure 1a; see the Supporting Information and Ref. [2b] for details). In this way, up to 1000 liposomes (Figures 1b–d),

[*] Dr. F. Höök
Department of Applied Physics
Chalmers University of Technology
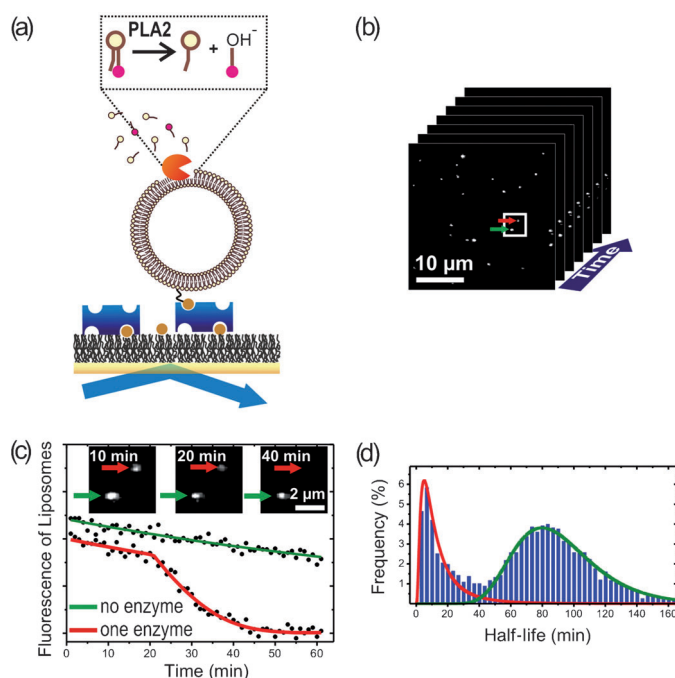41133 Göteborg (Sweden)
E-mail: Fredrik.hook@chalmers.se

Dr. M. Rabe, Dr. S. R. Tabaei
Department of Applied Physics
Chalmers University of Technology, Göteborg (Sweden)

Dr. H. Zetterberg
Sahlgrenska Academy at the University of Gothenburg
Mölndal (Sweden)

Dr. V. P. Zhdanov
Boreskov Institute of Catalysis, Russian Academy of Sciences
Novosibirsk (Russia)

Figure 1. Schematic of the single-liposome hydrolysis assay.[2b] a) The PLA2 activity is probed on surface-immobilized liposomes using total internal fluorescence (TIRF) microscopy (fluorescent dyes are attached to the lipids). b) Time-lapse images are acquired with a multitude of single liposomes from which individual substrate conversion kinetics are extracted. c) Due to the characteristic lag–burst behavior, the kinetic traces allow for an automated decision whether the liposome contains no enzyme (upper curve) or one enzyme (lower curve). In the "no enzyme" case the slow decrease of the signal is related to photobleaching. d) Histograms reveal the ratio between liposomes containing one enzyme (ca. 20%, red) and no enzyme (80%, green).

each processed by an individual membrane-associated PLA2, were measured in PLA2-containing human cerebrospinal fluid (CSF) samples, as described.[2b]

The observed kinetics can be treated in the framework of the conventional Michaelis–Menten mechanism [Eq. (1)], which was originally worked out for enzymes acting in solution.[9, 11] For membrane enzymes, the Michaelis–Menten reaction steps are usually complemented by those representing the enzyme and/or substrate transport to and association with the interface.[11] Certainly, such enzymatic reactions can also be complicated by other factors, such as complex lipid composition, raft formation, and curvature-induced membrane strain.[9, 12] Here, we consider the catalytic hydrolysis of lipids in a homogeneous liposome, where the substrate concentration, $[S] = N/N_0$, is defined by the current number (N) and initial number (N_0) of lipid molecules. The initial total internal reflection fluorescence (TIRF) intensity can be used to determine the liposome size and thus N for each liposome.[2b] If we apply Equation (2) for the reaction rate for hydrolysis by a single enzyme molecule, we have Equation (3).

$$\frac{\mathrm{d}N}{\mathrm{d}t} = -\frac{k_{\mathrm{cat}} N}{N + K_{\mathrm{m}} N_0} \tag{3}$$

Integration of Equation (3) yields Equation (4).

$$N - N_0 + K_{\mathrm{m}} N_0 \ln(N/N_0) = -k_{\mathrm{cat}}(t - t_0) \tag{4}$$

Here $t = t_0$ defines the start of the reaction after the lag time (Figure 1c). [Numerical calculations revealed excellent precision of the steady-state approximation represented by Eq. (3); see Figures S1 and S2 in the Supporting Information.] To use Equation (4), we take into account that the fluorescence of the lipid markers also decreases due to photobleaching. Since this process is independent of the enzymatic digestion, their kinetics are decoupled. Thus, the measurable number of lipid molecules containing a fluorescently active dye, N_1, is given by Equation (5).

$$N_1(t) = \alpha N(t) \exp(-k_{\mathrm{bl}} t) \tag{5}$$

Here α is the fraction of such lipids at $t = 0$, and k_{bl} is the photobleaching rate constant.

Equation (4) implies that the reaction half-life (i.e. the time corresponding to $N/N_0 = 1/2$) is approximately proportional to the initial number of lipid molecules N_0, and therefore to r^2, where r is the liposome radius. Additionally, the reaction under consideration exhibits a wide distribution of lag times prior to the enzymatic hydrolysis, and the Michaelis–Menten parameters may display explicit membrane-curvature dependence. Due to these factors, attempts to fit the ensemble-averaged kinetics directly by using Equation (4) with the average value of N_0 may result not only in quantitative errors but also in qualitatively incorrect conclusions even if the vesicle size distribution is narrow (as detailed below and Sections 5 and 6 in the Supporting Information). This further highlights the importance of measuring the reaction rate at the single-enzyme-molecule level in order to get accurate kinetic parameters. In addition, parameter estimates using Equation (4) become highly uncertain unless the experimental noise level is very low ($< 5\%$).[13]

To overcome these limitations, we propose a data analysis approach that combines the information of many single-enzyme kinetic data sets such that uncertainties caused by experimental noise and wide distribution in the onset time are eliminated, while unique features of single-enzyme kinetics are still available. Previous single-enzyme studies were also based on large data sets,[3–5] but they included multiple sequential measurements and thus relied on a relatively low rather than a statistically high number of enzyme molecules. The aforementioned strategy is optimal for characterizing specific enzymatic activity distributions; however, it is insufficient at rendering separate N_0 and Michaelis–Menten parameters, a feat made possible with our strategy.

The kinetic data can be transferred into a liposome-size- and lag-time-independent format, which enabled a coefficient of determination, the R^2 value [defined by Eq. (S11)],[14] to be calculated on discrete points of a tight mesh in the two-dimensional (k_{cat} and K_{m}) parameter space and plotted for each digested liposome as a contour map (right column in Figure 2). When roughly 1000 individual kinetic curves were used without superimposition of the distributions, k_{cat} and K_{m}
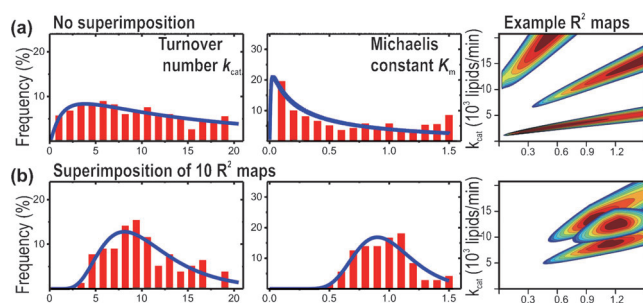
Figure 2. Determining the Michaelis constant and turnover number. Distributions of k_{cat} (left) and K_m (middle) obtained from a) ca. 1000 individual R^2 maps and b) sets of 10 superposed R^2 maps. The column on the right illustrates three typical examples of R^2 maps for each case. A wide distribution of individual R^2 maps is an indicator that accurate determination of the kinetic parameters is difficult.

values obtained from individual global maxima were widely spread, illustrating that the information contained in one single point in the k_{cat} and K_m parameter space is poor (left and middle graphs in Figure 2a). However, for 100 R^2 maps each composed of only 10 superimposed (single liposome) R^2 maps, the distributions of k_{cat} and K_m values become significantly more confined (left and middle graphs in Figure 2b). The superposition of cumulative numbers of individual R^2 maps thereby enables significantly more accurate parameter estimates. This was verified when we tested the ability of our strategy to accurately determine k_{cat} and K_m from an artificially produced set of data fulfilling Equation (3), to which real measured noise was added (see Figure S4 in the Supporting Information).

The magnitude of the error introduced by the shortcut offered by instead reducing experimental data by averaging over all kinetic curves prior to a determination of the parameters was shown to be as high as factor 2 to 3 (Figure 3). This is a direct consequence of the wide distributions in lag time and liposome size, and thus corresponds to the error that emerges in studies of this system using experimental methods that rely on ensemble averaging. While the influence of the liposomes size distribution (inset Figure 3a) on the enzyme kinetics can to some extent be handled by working with more narrow liposome size distributions, the significant error originating from the broad distribution in the lag time (inset Figure 3b) will inevitably remain. Hence, when ensemble averaging is employed, only an overall enzymatic activity of a sample can be measured, as was reported previously,[9,15] whereas extraction of the enzyme kinetic characteristics k_{cat} and K_m significantly benefits from analysis on the level of individual kinetic curves.

Further, with convergence in the determination of k_{cat} and K_m already from roughly 10 (single-liposome) R^2 maps (see Fig-

ure 2b) and that the size of each liposome can be deduced from the initial TIRF intensity,[2b] there appears a unique opportunity to investigate the dependence of k_{cat} and K_m on liposome size/membrane curvature. Indeed, the results obtained for PLA2 in CSF suggests that for large moderately curved liposomes the turnover numbers are significantly larger than for smaller liposomes with higher curvatures, while in contrast, the Michaelis constant decreases (Figure 4a). Similar results were obtained for purified PLA2 from *Naja naja* venom, with the difference that the dependence of K_m on curvature was not statistically significant (Figure S6). Artificial kinetics calculated using combined properties of the experimental noise and the initial size of a probed liposome revealed that artifacts resulting from different relative noise levels can indeed be excluded (Figure 4b).

The absolute values of k_{cat} and K_m determined here are in line with previously reported estimates on pig pancreas PLA2.[9] Previous studies[16] also suggest that PLA2-catalyzed lipid hydrolysis depends on membrane curvature, albeit without specifying the effect of curvature on k_{cat} and K_m. The dependence observed here is in line with that reported for other membrane-associated processes.[17] In principle, in analogy with the oligomerization of surface-bound proteins, the membrane curvature itself can influence reaction rates, at least if the liposome radius, R, is smaller than 25 nm.[18] We observe the effect for R up to 50 nm (Figure 4a and c). On this scale, the effect may be related to curvature-induced membrane strain.[12] The linear tensile strain of the external lipid layer is about $L/2R$, where L is the layer thickness. For $L = 2$ nm and $R = 50$ nm, the strain is 2%. In analogy with conventional catalytic processes,[19] this strain may result in up to a 10% change in the activation energy. With 1 eV as a scale of this energy, its change may be about 0.1 eV ($4\,kT$). Accordingly, the rates of processes occurring on liposomes with $R < 100$ nm may very well be up to about one order of
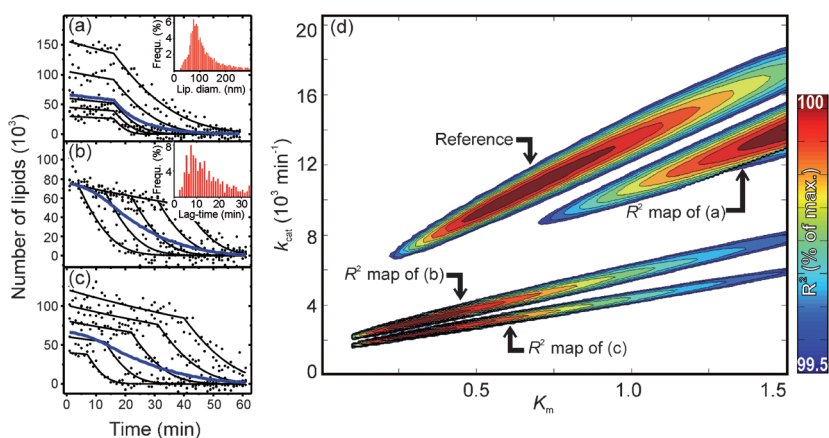
Figure 3. Errors originating from ensemble averaging. Examples of theoretically generated enzyme reaction kinetics without (solid black lines) and with experimental noise from human CSF samples (black circles) including a) the real size-distribution (see inset), b) the real lag-time distribution (see inset), and c) both. Blue curves represent ensemble averages generated from the kinetic data. Insets show histograms of the corresponding distributions of the size determined through the total fluorescence intensity of each liposome (a) and the lag time (b). d) R^2 maps for the examples (a) to (c) compared to the (correct) reference map with $k_{cat} = 10^4$ min^{-1} and $K_m = 0.6$.
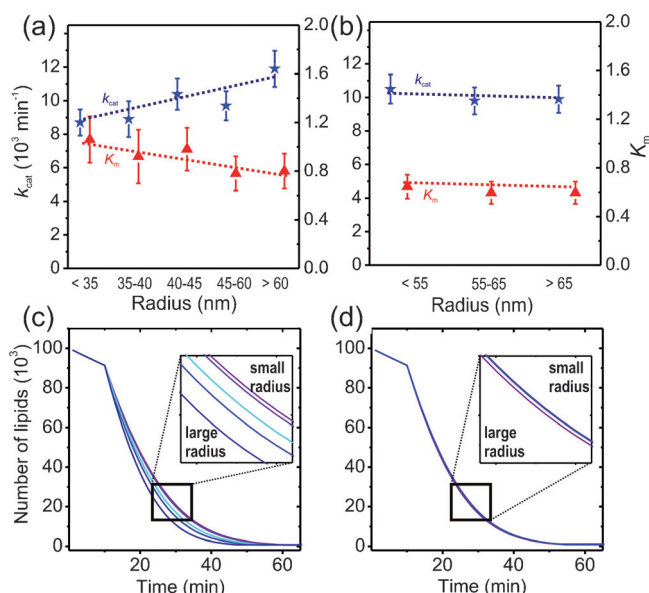
Figure 4. Liposome-size dependence of the enzyme-specific kinetic parameters. a) Estimated values of k_{cat} (stars) and K_m (triangles) versus liposome radius for PLA2 from human CSF samples. b) Control calculations using the kinetics generated with fixed k_{cat} and K_m values (right column). Panels (c) and (d) show the kinetics calculated (with fixed t_0) to illustrate the difference in the shape of digestion traces that correspond to the size dependence of the catalytic rate constants shown in panels (a) and (b), respectively.

magnitude faster or slower than on flat membranes. The effect we observe is weaker and accordingly can be explained by the membrane strain alone; however, product accumulation and phase separation causing curvature-dependent interfacial disorder and increased access for the enzyme to the cleavage site[16a] cannot be excluded.

To further quantify the accuracy and precision of the described data analysis procedure, we generated artificial kinetics with a known Michaelis constant and turnover number which in addition reflect the true experimental noise conditions of our data (see Figure S5). It turned out that the parameter estimates exhibited standard errors of 11% (k_{cat}) and 22% (K_m) when data sets of 100 individual kinetic curves (which approximately correspond to the number used to deduce the size dependence shown in Figure 3) were included. It is also instructive to consider the actual magnitude of the variation in the shape of the digestion curves caused by the size dependence of the catalytic rate constants deduced from the analysis. Figure 3c,d (and Figure S6b) shows digestion curves generated using Equation (4) and the rate constants shown in Figures 3a,b (and Figure S6a), respectively. The magnitude of these variations is indeed clearly visible but on the same order as the noise of the single-liposome digestion curves (Figure 3c). This thus further underpins the power of the single-vesicle data analysis approach presented in this work.

To conclude, the determination of enzyme-specific parameters is not as technically straightforward as one may assume at a first glance. The conventional approaches are based on examining the initial enzyme rates at varying initial substrate concentrations, and the recorded data are typically analyzed after transformation using a suitable linearization method, of which the best known is the Lineweaver–Burk plot.[13c] Since the number of data points is thereby limited by the number of measurements conducted with various substrate concentrations, it is common that parameter estimates can be far from the true values.[13b,c] The approach of the present work is different in that the key information is obtained not from initial enzyme rates at various initial substrate concentrations, but instead from the shape of the time-dependent product formation (see Figure 4c,d) at a constant initial substrate concentration and how this information is manifested in corresponding superimposed R^2 maps. Although the estimates of the Michaelis–Menten kinetic parameters are in our case quantitatively valid for hydrolysis of the membrane-embedded dye-labeled lipids only, the strategy is applicable to any type of single-enzyme kinetics. Its advantage is especially attractive for interfacial enzymes of the type explored herein, because it is typically very difficult to vary the substrate concentration with this class of enzymes. Concerning the precision of the parameter estimates, further improved statistics may aid a more detailed analysis of the observed membrane-curvature dependence of the enzyme-specific Michaelis–Menten parameters. Such studies would also benefit from direct label-free visualization of individual liposomes,[20] which could offer a means to deduce whether there is an influence on the measured enzymatic kinetics of the dye-labeled lipids and also open up for extensions including studies addressing the influence of lipid composition on digestion kinetics, as previously addressed using ensemble-averaging approaches.[9] Regarding these aspects, it is interesting to note that PLA2 and related membrane-associated enzymes are biomarkers for a range of diseases,[1b, 21] and have emerged as potential drug targets,[22] and also participate in the innate immune response by acting as potent antimicrobial agents.[23] The membrane-curvature-dependent enzyme kinetics may thus suggest that both lipid composition[24] and membrane morphology contribute to their corresponding functions. Further, from a pharmaceutical perspective, our approach may offer a new means to determine whether inhibitory drugs designed to alter the enzyme activity primarily influence k_{cat}, K_m, or both, information that was previously unattainable for this class of enzymes.

[1] a) W. E. Moerner in *Single Molecule Spectroscopy in Chemistry, Physics and Biology, Vol. 96* (Eds.: A. Graslund, R. Rigler, J. Widengren), Berlin, Springer, **2010**, pp. 25–60; b) E. Kaiser, *Crit. Rev. Clin. Lab. Sci.* **1999**, *36*, 65–163.

[2] a) H. H. Gorris, D. R. Walt, *Angew. Chem. Int. Ed.* **2010**, *49*, 3880–3895; *Angew. Chem.* **2010**, *122*, 3970–3986; b) S. R. Tabaei, M. Rabe, H. Zetterberg, V. P. Zhdanov, F. Hook, *J. Am. Chem. Soc.* **2013**, *135*, 14151–14158.

[3] a) H. P. Lu, L. Y. Xun, X. S. Xie, *Science* **1998**, *282*, 1877–1882; b) B. P. English, W. Min, A. M. van Oijen, K. T. Lee, G. B. Luo, H. Y. Sun, B. J. Cherayil, S. C. Kou, X. S. Xie, *Nat. Chem. Biol.* **2006**, *2*, 87–94.

[4] a) L. Edman, Z. Foldes-Papp, S. Wennmalm, R. Rigler, *Chem. Phys.* **1999**, *247*, 11–22; b) W. Min, B. P. English, G. B. Luo, B. J. Cherayil, S. C. Kou, X. S. Xie, *Acc. Chem. Res.* **2005**, *38*, 923–931.

[5] a) D. M. Rissin, H. H. Gorris, D. R. Walt, *J. Am. Chem. Soc.* **2008**, *130*, 5349–5353; b) Y. K. Choi, I. S. Moody, P. C. Sims, S. R. Hunt, B. L. Corso, I. Perez, G. A. Weiss, P. G. Collins, *Science* **2012**, *335*, 319–324; c) Z. Xie, N. Srividya, T. R. Sosnick, T. Pan, N. F. Scherer, *Proc. Natl. Acad. Sci. USA* **2004**, *101*, 534–539.

[6] a) D. Ringe, G. A. Petsko, *Science* **2008**, *320*, 1428–1429; b) M. Garcia-Viloca, J. Gao, M. Karplus, D. G. Truhlar, *Science* **2004**, *303*, 186–195; c) D. Aili, M. Mager, D. Roche, M. M. Stevens, *Nano Lett.* **2011**, *11*, 1401–1405.

[7] R. Coleman, *Biochim. Biophys. Acta Rev. Biomembr.* **1973**, *300*, 1–30.

[8] M. K. Jain, B. Z. Yu, J. Rogers, G. N. Ranadive, O. G. Berg, *Biochemistry* **1991**, *30*, 7306–7317.

[9] O. G. Berg, B. Z. Yu, J. Rogers, M. K. Jain, *Biochemistry* **1991**, *30*, 7283–7297.

[10] S. A. Tatulian, *Biophys. J.* **2001**, *80*, 789–800.

[11] M. K. Jain, O. G. Berg, *Biochim. Biophys. Acta Lipids Lipid Metab.* **1989**, *1002*, 127–156.

[12] V. P. Zhdanov, F. Hook, *Biophys. Chem.* **2012**, *170*, 17–24.

[13] a) R. G. Duggleby, *Biochim. Biophys. Acta, Protein Struct. Mol. Enzymol.* **1994**, *1205*, 268–274; b) G. L. Atkins, I. A. Nimmo, *Anal. Biochem.* **1980**, *104*, 1–9; c) J. E. Dowd, D. S. Riggs, *J. Biol. Chem.* **1965**, *240*, 863–869.

[14] T. O. Kvalseth, *Am. Stat.* **1985**, *39*, 279–285.

[15] S. Chalbot, H. Zetterberg, K. Blennow, T. Fladby, I. Grundke-Iqbal, K. Iqbal, *Clin. Chem.* **2009**, *55*, 2171–2179.

[16] a) C. Leidy, O. G. Mouritsen, K. Jorgensen, N. H. Peters, *Biophys. J.* **2004**, *87*, 408–418; b) M. Menashe, G. Romero, R. L. Biltonen, D. Lichtenberg, *J. Biol. Chem.* **1986**, *261*, 5328–5333; c) D. Lichtenberg, G. Romero, M. Menashe, R. L. Biltonen, *J. Biol. Chem.* **1986**, *261*, 5334–5340.

[17] a) B. Antonny, *Annu. Rev. Biochem.* **2011**, *80*, 101–123; b) T. Baumgart, B. R. Capraro, C. Zhu, S. L. Das, *Annu. Rev. Phys. Chem.* **2011**, *62*, 483–506; c) G. Drin, J. F. Casella, R. Gautier, T. Boehmer, T. U. Schwartz, B. Antonny, *Nat. Struct. Mol. Biol.* **2007**, *14*, 138–146; d) N. S. Hatzakis, V. K. Bhatia, J. Larsen, K. L. Madsen, P. Y. Bolinger, A. H. Kunding, J. Castillo, U. Gether, P. Hedegard, D. Stamou, *Nat. Chem. Biol.* **2009**, *5*, 835–841.

[18] M. Kurylowicz, H. Paulin, J. Mogyoros, M. Giuliani, J. R. Dutcher, *J. R. Soc. Interface* **2014**, *11*, 20130818..

[19] M. Mavrikakis, B. Hammer, J. K. Norskov, *Phys. Rev. Lett.* **1998**, *81*, 2819–2822.

[20] J. Andrecka, K. M. Spillane, J. Ortega-Arroyo, P. Kukura, *ACS Nano* **2013**, *7*, 10662–10670.

[21] G. Y. Sun, P. B. Shelat, M. B. Jensen, Y. He, A. Y. Sun, A. Simonyi, *Neuromol. Med.* **2010**, *12*, 133–148.

[22] a) V. Magrioti, G. Kokotos, *Expert Opin. Ther. Pat.* **2010**, *20*, 1–18; b) R. C. Reid, *Curr. Med. Chem.* **2005**, *12*, 3011–3026.

[23] T. J. Nevalainen, G. G. Graham, K. F. Scott, *Biochim. Biophys. Acta Mol. Cell Biol. Lipids* **2008**, *1781*, 1–9.

[24] K. A. Brogden, *Nat. Rev. Microbiol.* **2005**, *3*, 238–250.